Journal of Manufacturing Processes 133 (2025) 1196–1206

Contents lists available at ScienceDirect

Journal of Manufacturing Processes

journal homepage: www.elsevier.com/locate/manpro

Solvent-assisted rapid manufacturing of free-form soft polymer structures with hierarchical pores

Smruti Parimita [a], Umamaheshwari Ravikumar [b], Hariharan Krishnaswamy [a,e], Pijush Ghosh [c,d,*]

[a] Manufacturing Engineering Section, Department of Mechanical Engineering, IIT Madras, Chennai 600036, India
[b] National Centre for Nanoscience and Nanotechnology, University of Madras, Chennai, 600025, India
[c] Department of Applied Mechanics and Biomedical Engineering, Indian Institute of Technology Madras, Chennai 600036, India
[d] Centre for Soft and Biological Matter, Indian Institute of Technology Madras, Chennai 600036, India
[e] Additive Manufacturing Research Group, Indian Institute of Technology Madras, Chennai 600036, India

ARTICLE INFO

Keywords:
Phase separation
Under solvent
Porous
Free-form structures
Direct ink writing
Printability
Soft biopolymer

ABSTRACT

Despite recent advancements in 3D printing, the fabrication of three-dimensional tubular structures with soft materials remains challenging due to the difficulty of maintaining shape fidelity in the printed structures. Here, we designed and printed porous tubular structures based on Liquid–Liquid Phase Separation (LLPS) in a tertiary system via Direct Ink Writing (DIW). The main highlight of this work lies in the approach that incurs the 3D printing of soft polymers in the solution phase in a liquid bath that is miscible with the solvent ink but immiscible with the polymer. This leads to spontaneous solidification, resulting in structures with hierarchical internal porosity using different polymer concentrations. A ternary phase diagram was established to determine the solvent-polymer-nonsolvent composition that can potentially undergo a phase separation during the process of printing. Further to the selection of composition, rheological analysis of the solution corresponding to the composition was performed to understand their suitability for printing. The ternary diagram also helped in choosing the appropriate composition for obtaining the necessary pore characteristics of the printed structures. The idea of omnidirectional printing inside a suspension gel medium also helped to fabricate free-form complex shapes without any additional physical support. This work, therefore, provides a simple route to fabricate 3D free-form structures of a soft polymer, which can serve as a useful technique for DIW-based fabrication of soft robotic components and flexible wearable devices, as well as in-vivo organ and scaffold printing.

1. Introduction

Additive manufacturing, or 3D printing, has evolved into a versatile technique for creating complex, functional 3D structures from a variety of materials, including metals [1], ceramics [2], and polymers [3]. The advancement of 3D printing technology has made it possible to directly manufacture functional soft structures, particularly for soft polymer materials with complex polymerization properties [4]. However, 3D printing and the use of soft polymers are still in their infancy. Previous research has identified a number of challenges including a limited choice of printable materials, poor printing resolution and speed for direct-ink writing, and inferior functionalities [5,6]. Therefore, new emerging approaches must be developed to release the enormous potential of 3D printing of soft polymers.

Soft polymer structures with tailored porous architecture have unique advantages for developing a variety of applications including lightweight structures [7], vibration-absorptive materials [8], catalyst supports [9], tissue scaffolds [10] and for controlled release of drugs [11]. Porosity in tissue engineering affects cell adhesion, migration, and proliferation, as well as the mechanical integrity of the tissue scaffolds [12,13]. Highly porous structures are crucial as they support and facilitate the uniform distribution of cells. However, it reduces the overall strength of the scaffold [14–16]. Therefore, it is necessary to optimize the mechanical strength and porosity to achieve an optimal balance. Apart from conventional techniques (phase separation, freeze-drying, salt leaching, emulsification), several strategies, including some basic methods (control over sol–gel and post-processing strategies) and various templating methods, have been reported to fabricate porous structures [17]. These methods have been useful for fabricating materials with a wide range of porosity from 1 μm to 100 μm. However, fabricating intricate architecture using the above methods requires the design and fabrication of complex moulds. Furthermore, the parameters of these moulding techniques exhibit complex relations with the porosity that is not practical to engineer the desired porous structure easily.

* Corresponding author at: Department of Applied Mechanics and Biomedical Engineering, Indian Institute of Technology Madras, Chennai 600036, India.
E-mail address: pijush@iitm.ac.in (P. Ghosh).

https://doi.org/10.1016/j.jmapro.2024.11.065
Received 2 September 2024; Received in revised form 24 October 2024; Accepted 21 November 2024
Available online 12 December 2024

Although studies have demonstrated that porous structures may be created directly through the 3D printing process [18], these pores are often macroscopic, which further restricts the control over the total porosity. Alternatively, a creative approach to get around the above problem and get porosity over multiple length scales is to print composites packed with removable particles/components and then remove these sacrificial components. However, the removal of these sacrificial components is a challenge for geometrically complex structures.

Liquid–Liquid Phase Separation (LLPS) is one of the various processes available for designing and developing porous polymer films employing soft polymer materials [19,20]. This process is easier, quicker, less expensive, and more adaptable in terms of material selection and control over the shape of the porous polymer matrix. The LLPS technique involves maintaining a homogenous polymer-solvent-nonsolvent combination at a fixed temperature and humidity for complete diffusion of both solvent and nonsolvent. Generally, the mixture is selected such that the rate of diffusion of solvent is faster than that of nonsolvent. This leads to an increase in the concentration of nonsolvent in the mixture. As a result, two different phases emerge: the polymer-rich phase and the polymer-lean phase. While the polymer-lean phase, which is rich in nonsolvent, creates pores in the matrix, the polymer-rich phase forms the solid film or matrix [21]. Depending on combinations of mixture and environmental conditions, a polymer matrix with varying pore morphologies can be obtained [22]. Structures with asymmetric, symmetric, and hierarchical pores can be prepared using this technique. This technique has been widely exploited for casting thin films/ membranes for applications in photonics [23], cell cultivation [24], energy storage and conversion [25], and drug delivery [26].

Direct Ink Writing (DIW)is one of the versatile LLPS-based 3D printing techniques for fabricating soft structures. Attempts have been made in the recent past to print complex structures in a suspension bath medium using embedded ink writing [27,28]. It is of interest to understand the mechanism of 3D printing of soft polymers using LLPS and for further exploration to fabricate complex structures.

This work presents the application of direct ink writing 3D printing utilizing LLPS. A suspension medium (bath) in DIW 3D printing was employed to solidify the printed ink by extracting the solvent through LLPS, resulting in porous structures. We performed DIW 3D printing of TPU with DMF as a solvent in a water-based suspension media (as a non-solvent). A detailed study was investigated using a ternary phase diagram to understand the influence of polymer-solvent-nonsolvent composition on the printability of ink. The printability of different architectures was analysed by varying the concentration of TPU. This method is a one-step fabrication process to achieve complex hierarchical porous structures embedded in TPU. The mechanical strength of the structures can be modulated by the inclusion of pores within a single material system and also finds application in cell culture [12,13], tissue engineering scaffolds [14–16], and components for EMI shielding [29,30]. This study provides insight and guidelines to identify different processing parameters required for the successful 3D printing of complex architectures from soft polymer based on LLPS.

2. Materials and methodology

The thermoplastic granules with shore hardness 92 A (LARIPUR LPR 9020) were purchased from Anoopam India Pvt. Ltd. All the chemicals and reagents, i.e., N, N- Dimethyl formamide (DMF) and carboxymethyl cellulose powder were purchased from SRL Chemicals Pvt. Ltd.

2.1. Preparation of printing inks

The ink was prepared using different compositions (10 to 70 w/v % with a regular interval of 10) of thermoplastic polyurethane (TPU) granules in N, N- Dimethyl formamide (DMF) as solvent. The TPU granules were added to DMF solvent and mixed homogeneously for 4 h using a mechanical stirrer at a temperature of 80 °C. The TPU ink was centrifuged at 3000 rpm for 15 min to remove the air bubbles. The acrylic colour was added to the ink for better visibility during printing.

2.2. Preparation of supporting media (bath)

To improve the efficiency of 3D printing of soft polymer, a suspension media was used for under bath printing of low viscous ink. Water and water-based suspension media were used as non-solvent for the TPU-DMF model ink. DI water was used as a suspension medium for rapid curing action. The polymer-solvent(TPU-DMF) demixing in the polymer-solvent-non-solvent(TPU-DMF-water) was analysed using titration method and explained using a ternary phase diagram. The carboxymethyl cellulose(CMC) gel was prepared as supporting media by adding different compositions(1%–6% w/v) of CMC in DI water. The desired concentration of CMC powder was added to deionized (DI) water. The dispersion was then mixed homogeneously using a mechanical stirrer at 1000 rpm to completely wet the CMC particles. The gel was then degassed to remove the air bubbles. The vat containing supporting media was kept in a desiccator, and a negative pressure was applied for 2–3 h to remove the air bubbles.

2.3. Viscoelastic characterization of printing inks and supporting media

Rheological characterizations were conducted to study the printability of the TPU ink in suspension media. The viscosity of the polymer inks was determined using a rotational rheometer (MCR301, Anton Paar, Austria) using a 25 mm parallel plate with a measurement gap of 1 mm. To study the shear-thinning property, the viscosity of the tested TPU ink was measured at shear rates ranging from 0.1 to 1000 s^{-1}. DI water and CMC gel were used as suspension media. A rheometer was used to characterize the steady-state shear viscosity (as explained above). Strain sweeps from 0.1% to 1000% at a frequency of 1 Hz was performed to determine the storage and loss moduli. All rheological characterization was carried out at ambient temperature (25 °C) and under atmospheric pressure (the working temperature of the 3D printer).

2.4. Set-up for rapid liquid printing in supporting medium

A custom-built design direct-ink writing(DIW) 3D printer was used for printing the samples. The flatbed was replaced with a vat containing the supporting media for the under-bath printing (as shown in Fig. 1). The TPU ink of different concentrations were loaded into a 50 ml syringe and mounted to the printer head. A 15G nozzle with an inner diameter of 1.5 mm and 50 mm gauge length was used for printing inside the supporting media.

Two printing strategies were adopted, layer-by-layer and free-form building. The former approach utilized 'SolidWorks™' to build the part geometry and 'Ultimaker Cura' to slice the layers. The free-form printing is continuous wherein the printing trajectories were generated using 'SolidWorks™'. These trajectories were discretized into points and constructed to G-code using 'Matlab™' software.

2.5. Evaluation of printed ink patterns in suspension medium

The performance was studied by printing a 20 mm straight line with different concentrations of TPU ink inside the suspension medium. A parametric study was performed, the details of which are tabulated in Table 1. The parametric range in Table 1 is based on successful printing during preliminary studies. The interface bonding between multiple layers was evaluated by printing a grid-like structure. All the printing was independently repeated at least three times. All images and videos of the experiments were captured in real-time (using a 64megapixel camera, resolution of 1440 * 1440 and at a rate of 30 fps).

After printing, the structure was immersed in the supporting media for 30 min to guarantee that the solvent from the polymer ink had been entirely removed. The residence duration of the printed object in the supporting media was measured by manually monitoring its solidification at various time intervals and characterized by thermogravimetric analysis (TGA)(explained in supplementary section S2). The printed samples were washed with DI water and dried for further analysis.

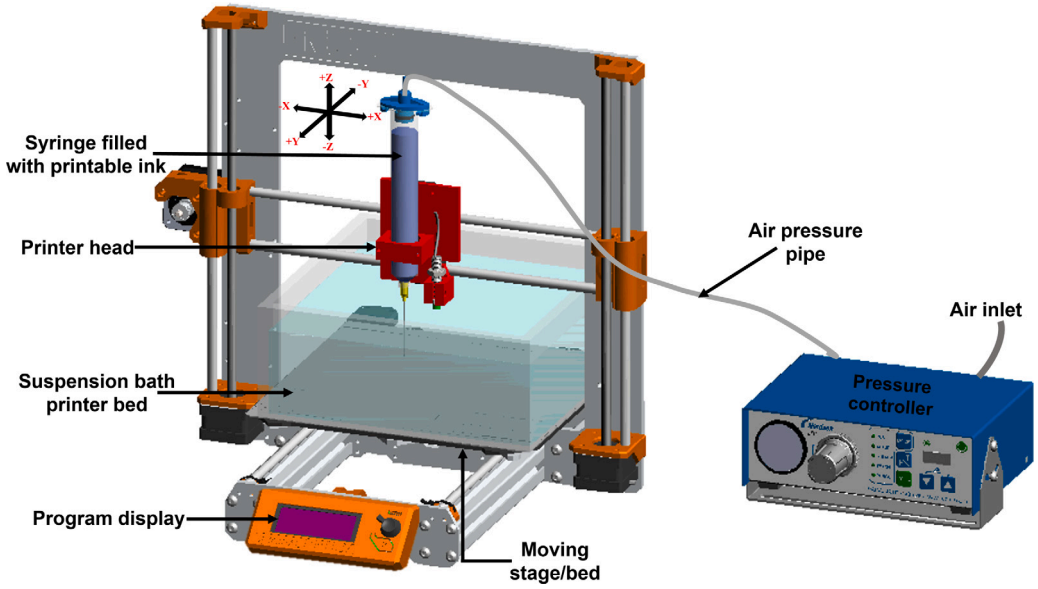

Fig. 1. A schematic representation of the custom-built design direct-ink writing(DIW) 3D printer for rapid liquid printing in supporting medium.

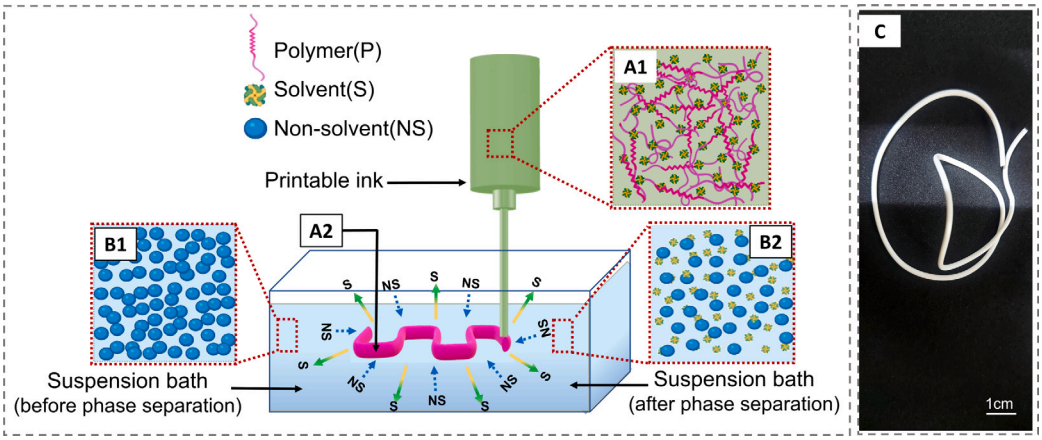

Fig. 2. Schematic illustration of printing the structure inside a suspension bath medium using a direct-ink writing 3D printer.

Table 1
Optimized printing parameters for printing TPU structures in suspension media.

Parameter	Value	Unit
Concentration of TPU, TPU_n	n = 20,30,40,50,60	%(w/v)
Concentration of CMC, CMC_n	n = 1.0,2.0,3.0,4.0,5.0,6.0	%(w/v)
Extrusion pressure, P	1,2,3,4,5	bar
Printing speed, S	1,2,3,4,5	mm/s
Diameter of a nozzle, d	1.5	mm

2.6. Pore characterization

A field emission scanning electron microscope (Inspect F50 from FEI) operating at 5 kV was used to analyse the microscopic morphology of the 3D printed samples. The sample specimens were sputter coated with a thin gold layer using an ion coater (Hitachi E-1300) for 120 s prior to SEM analysis.

3. Results and discussion

The goal of this research is to create a simple method for fabricating porous freeform objects out of soft thermoplastic polymer. The suspension media applied in this method acts as a chemical environment for the rapid solidification of the 3D structures, as well as it provides physical support to the free-form structures. The rapid solidification is achieved by Liquid–Liquid Phase Separation (LLPS). The process of rapid solidification also leads to hierarchical 3D porous structures, which can be engineered, as explained later. As schematically represented in Fig. 2, 'A1' represents the polymer ink, which is a mixture of TPU (polymer) and DMF (solvent). Once 'A1' is extruded into a suspension medium ('B1') consisting of water (non-solvent), 'A1' solidifies to 'A2' through the mechanism of LLPS. After the phase separation, the component 'B1' transforms to a mixture ('B2') of both DMF and water. The component 'A2' contains a mixture of 'polymer-rich' and 'polymer-lean' phases, whose mechanism is explained in detail in the next section. Upon extraction of solvents from 'A2', the solidified component 'C' is obtained. Manipulation of 'polymer-rich' and 'polymer-lean' phase composition along with phase kinetics leads to different characteristics of 'C', as elaborated in the subsequent section.

3.1. Exploring the role of phase separation in 3D printing

Liquid–liquid Phase Separation(LLPS) is considered to be the driving mechanism for the rapid solidification process of the polymer ink 'A' to obtain the solidified printed strand 'C' as shown in Fig. 2. The mechanism of rapid solidification is well explained through the phase

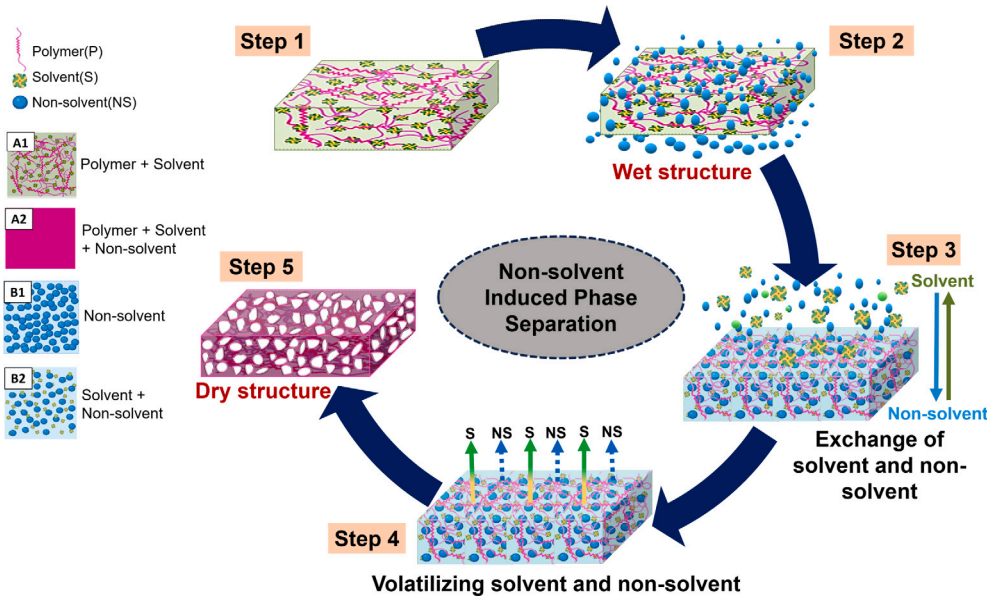

Fig. 3. Schematic illustration of liquid–liquid phase separation mechanism resulting in rapidly cured porous structures.

separation in the literature [31]. Phase separation technique has been frequently used to form polymer thin films and membranes [32]. In phase separation, a polymer is fabricated from a solution state to a solid state in a controlled way. In this work, the LLPS technique was employed, as the ink and suspension media are categorized as Newtonian or non-Newtonian fluids, respectively. Phase separation in LLPS occurs in a ternary mixture composed up of non-solvent, solvent, and polymer. The polymer film/matrix experiences a diffusion-driven exchange of solvent and non-solvent due to the miscibility of the non-solvent with the solvent of the polymer solution. At a certain non-solvent concentration, the polymer solidifies (the solid structure is termed as matrix in the rest of the manuscript) as illustrated in Fig. 3 and in supplementary video SV1.

The mechanism responsible for the matrix formation is governed by a number of parameters [31]. Using a ternary diagram created with the help of the extended Flory–Huggins theory, Denolf et al. [32] demonstrated how different factors interact to cause phase separation, and then experimentally validated using the titration method. A calculation of the molar Gibbs free energy of mixing for ternary systems was made using this theory:

$$\frac{\Delta G_m}{RT} = n_1 \ln \varphi_1 + n_2 \ln \varphi_2 + n_3 \ln \varphi_3 + g_{12}(u_2) n_1 \varphi_2 + \chi_{13} n_1 \varphi_3 + \chi_{23} n_2 \varphi_3 + \chi_{123} n_1 \varphi_2 \varphi_3 \quad (1)$$

where R(J/mol*K) is the universal gas constant, T(K) the absolute temperature, and the volume fraction and number of moles are represented by φ_i and n_i respectively, with i referring to nonsolvent(1), solvent(2) or polymer(3). In Eq. (1), the binary interaction parameters are g_{12} between the solvent and the nonsolvent, χ_{13} between the nonsolvent and polymer, and χ_{23} between the solvent and polymer. It was assumed that only g_{12} is concentration dependent, expressed as a function of $u_2 = \varphi_2/(\varphi_1+\varphi_2)$, while χ_{13} and χ_{23} was considered constant. Moreover, χ_{123} represented the ternary interaction parameter between the three system components. This parameter was used to characterize non-trivial phenomena, such as the polymer's solubility being higher or lower than predicted based on binary interaction parameters. It was reported that the binodal curve moves towards the polymer–solvent axis when g_{12} decreases or when χ_{13} or χ_{23} increases. An increased affinity between the solvent and the nonsolvent resulted in a narrower single-phase region. In contrast, an increased affinity between the polymer and the solvent or nonsolvent resulted in a larger single-phase region.

This study provided insights into the selection of suitable solvents and non-solvents for phase separation. Therefore, it is evident from the study that the concentration and interaction parameters of polymer, solvent, and nonsolvent play a significant role in the phase separation mechanism.

The morphology of the polymer matrix is influenced by the varying interactions of solvent/non-solvent. Increasing the ratio of water/PMMA at the point of phase separation resulted in an increase in porosity. While the porosity decreased with an increase in temperature [19]. Even the morphology could be tailored from non-porous film (60% RH) to porous film with an increase in relative humidity (74% RH). The concentration of polymer and nonsolvent had a significant influence on the pore size, as reported elsewhere [33].

The polymer solution becomes thermodynamically unstable upon exposure to the non-solvent. Two coexisting liquid phases that are in thermodynamic equilibrium separate from the polymer solution. The polymer-rich phase eventually solidifies to create a solid matrix, whereas the non-solvent-rich polymer-lean phase finally forms the pores in the matrix. The steps of the LLPS of a polymer/solvent/non-solvent system are illustrated in Fig. 3. Step 1 represents a system 'A1' containing a mixture of TPU (polymer)and DMF (solvent). When the system 'A1' comes in contact with system 'B1' containing non-solvent in step 2, an exchange of solvent and non-solvent between 'A1' and 'B1' happens. This results in a decrease in the concentration of the solvent and an increase in that of the non-solvent in the system 'A1'(as shown in step 3). This causes the polymer solution to split into two phases at equilibrium: a rich polymer phase and a poor or lean polymer phase. Upon evaporating/volatilizing the solvent and non-solvent from system 'A1'(shown in step 4), the polymer-rich phase solidifies to a stable structure 'C,' and the polymer-lean phase results in the formation of pores in the system 'C'. This results in the formation of a porous membrane structure, as shown in step 5.

This method of forming stable solid structures is used in 3D printing of porous structures using LLPS. The selection of a solvent-non-solvent system, the composition of the polymer solution, the composition of the coagulation bath, and the printing parameters are the main variables that affect LLPS 3D printing. The choice of the solvent-nonsolvent system have an influence on the morphology of the printed structure, mechanical properties, and interlayer characteristics. The polymer must be dispersible in the solvent of choice, and the solvent and nonsolvent must be soluble. More solvent and non-solvent miscibility increases

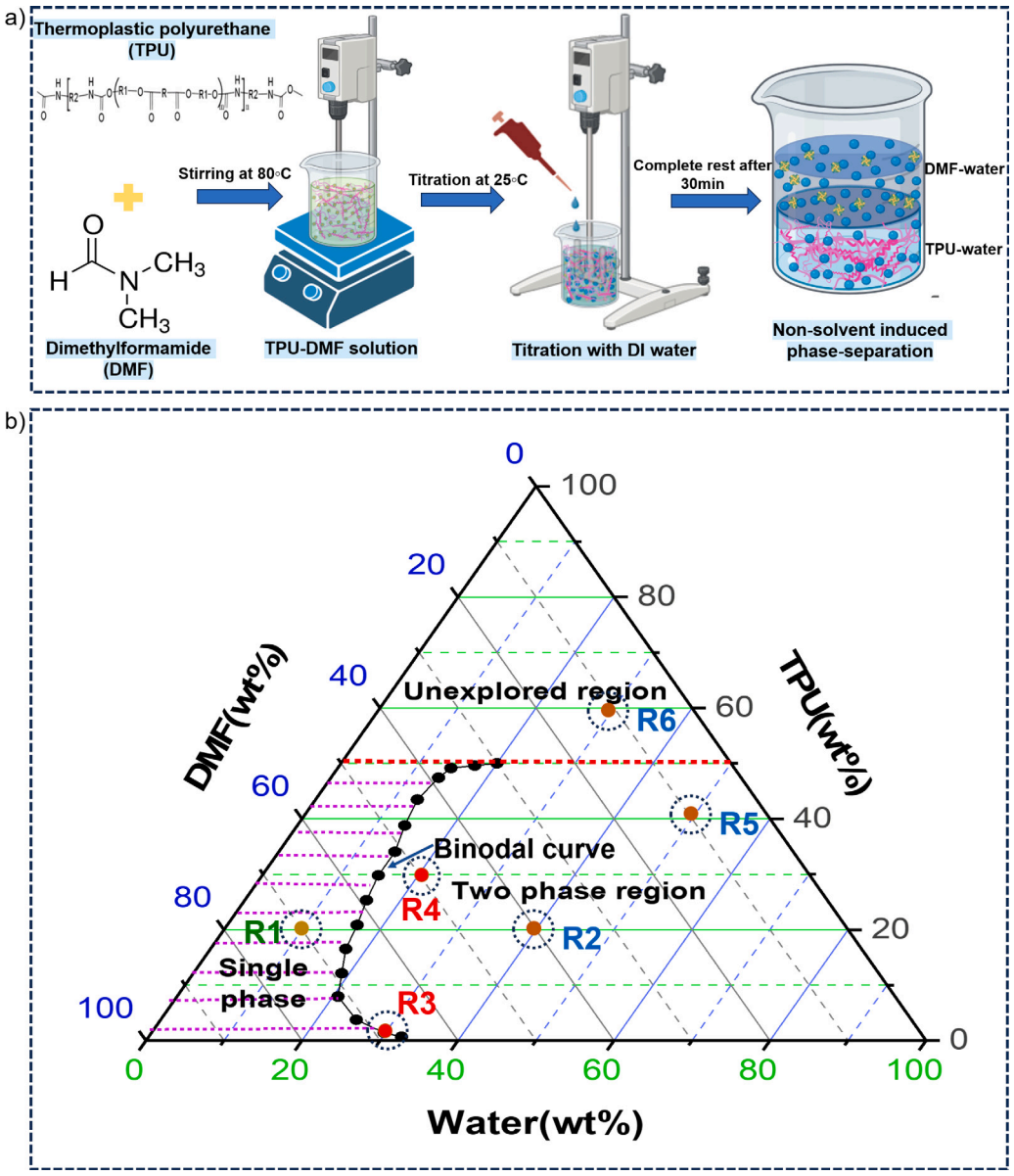

Fig. 4. (a) Process layout to obtain cloud point using titration method, (b)The phase diagram of TPU-DMF-H_2O system at 25 °C, the cloud-points are represented using solid circle. A binodal curve was obtained using a solid line connecting the cloud points. The single-phase region was represented by shaded lines, and the two-phase region was at the right of the binodal curve. The cloud points could not be determined experimentally for the region above the horizontal dotted line with polymer concentrations above 50% due to their high viscosity.

the likelihood of instantaneous demixing, which creates a more porous structure. When mutual affinity is low, an asymmetric structure with a dense, non-porous top layer is most likely formed. In LLPS, the polymer chosen restricts the solvents and non-solvents that may be employed in the phase separation process. Furthermore, the solvent, along with polymer concentration, plays an important role in the development of printed structures. The polymer concentration in the solution is a critical parameter affecting the morphology of the printed structures. At the non-solvent interface, the concentration of polymers increases as the polymer concentration in the solution increases. This indicates lower porosity as polymer concentration reduces the rate of phase separation.

3.2. Development and application of ternary phase diagram

A ternary phase diagram was constructed for the TPU-DMF-H_2O system. Fig. 4a shows the steps followed to obtain cloud point using titration at 25 °C, and Fig. 4b illustrates the phase diagram obtained thereof. For this purpose, TPU in DMF solutions with concentrations ranging between 1 and 50% w/v were prepared by mixing a necessary amount of TPU granules and DMF in a beaker. Deionized (DI) water was then added dropwise with a micro syringe into the beaker until the solution became turbid. The rate of non-solvent addition to the solution was regulated until the solution became homogenous between two successive additions. The turbid solution was gently agitated for several hours until phase separation was achieved. Finally, gravimetry was used to determine and report the composition of the turbid solution. Under this condition, the solution turned milky upon further addition of non-solvent, and the separated phases became substantial, signifying entry into the two-phase region.

The vertices of the phase diagram (Fig. 4b) represent the three components. The ternary system is a component of two-phase fields; single and two-phase regions. In Fig. 4b, the single-phase region where the mixture is in the solution state is represented by the shaded area.

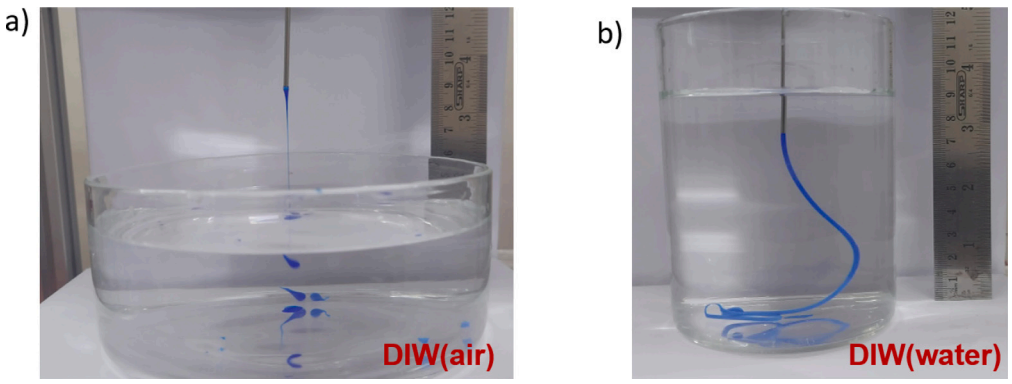

Fig. 5. (a) The extrusion of low-viscosity inks of TPU did not form continuous filaments but formed droplets in the air, (b)whereas the same ink formed a continuous filament in water (the composition corresponds to point R2 in the phase diagram).

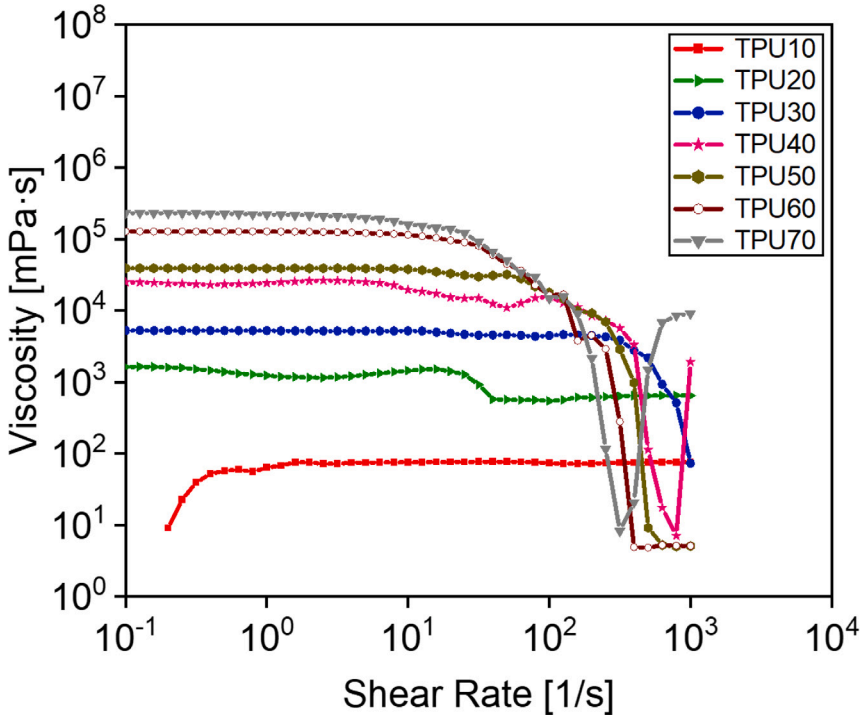

Fig. 6. A printable TPU-DMF ink showing shear thinning ability.

The phase field boundary delimiting the liquid–liquid demixing is known as the binodal curve [21]. The solid circles (in black) in the phase diagram represent the cloud points (obtained from the titration experiment) that form the binodal curve between single and two-phase regions. According to Denolf et al. [32], the binodal curve gives information on the minimal theoretical amount of polymer, solvent, and nonsolvent needed to start precipitation, assuming equilibrium conditions. Different compositions of TPU from 0.5%–70% w/v were explored to analyse the matrix formation. The construction of the phase diagram was limited to 50% w/v TPU, as the viscosity of the solution $\geq$ 100000 mPa s, was too high to measure the cloud point through titration. A detailed study was carried out by arbitrarily choosing different combinations of polymer and solvent systems from the ternary phase diagram to explore the printability of the ink through phase separation in the next section.

3.3. Printable ink for LLPS

In order to relate the printability with the phase separation mechanism, four arbitrary points (with different compositions of ink) were chosen from the ternary phase diagram. It was well understood that the phase separation rate and the solidification rate during printing can be altered to fabricate structures with different pore sizes and porosity by altering the polymer and solvent concentration. The composition (20,70,10)(R1 in Fig. 4) cannot be printed as it lies in the single-phase region. Selected compositions (R2, R3, R4, R5, and R6) lying in the two-phase regions were evaluated for printability. Point R2 (20,40,40) contains enough non-solvent for the phase separation and can be used for 3D printing. Although R3 (2,68,30) lies in the two-phase region, it was difficult to print due to very low viscosity, which resulted in the formation of discontinuous filaments upon extrusion in a water bath. Point R2 (20,40,40) formed discontinuous filaments in the air whereas formed continuous filaments in the water bath(shown in Fig. 5(a)).

Although points R4 (30,50,20), R5 (40,10,50), and R6 (60,10,30) are in the two-phase region, the printability is governed by rheological characterization.

The rheological behaviour of TPU ink from 10%–70% w/v (10% w/v TPU is represented as TPU10 and the same for other compositions) was studied from the steady-shear plots. The plot displayed a Newtonian behaviour for TPU10 and TPU20, while a shear-thinning

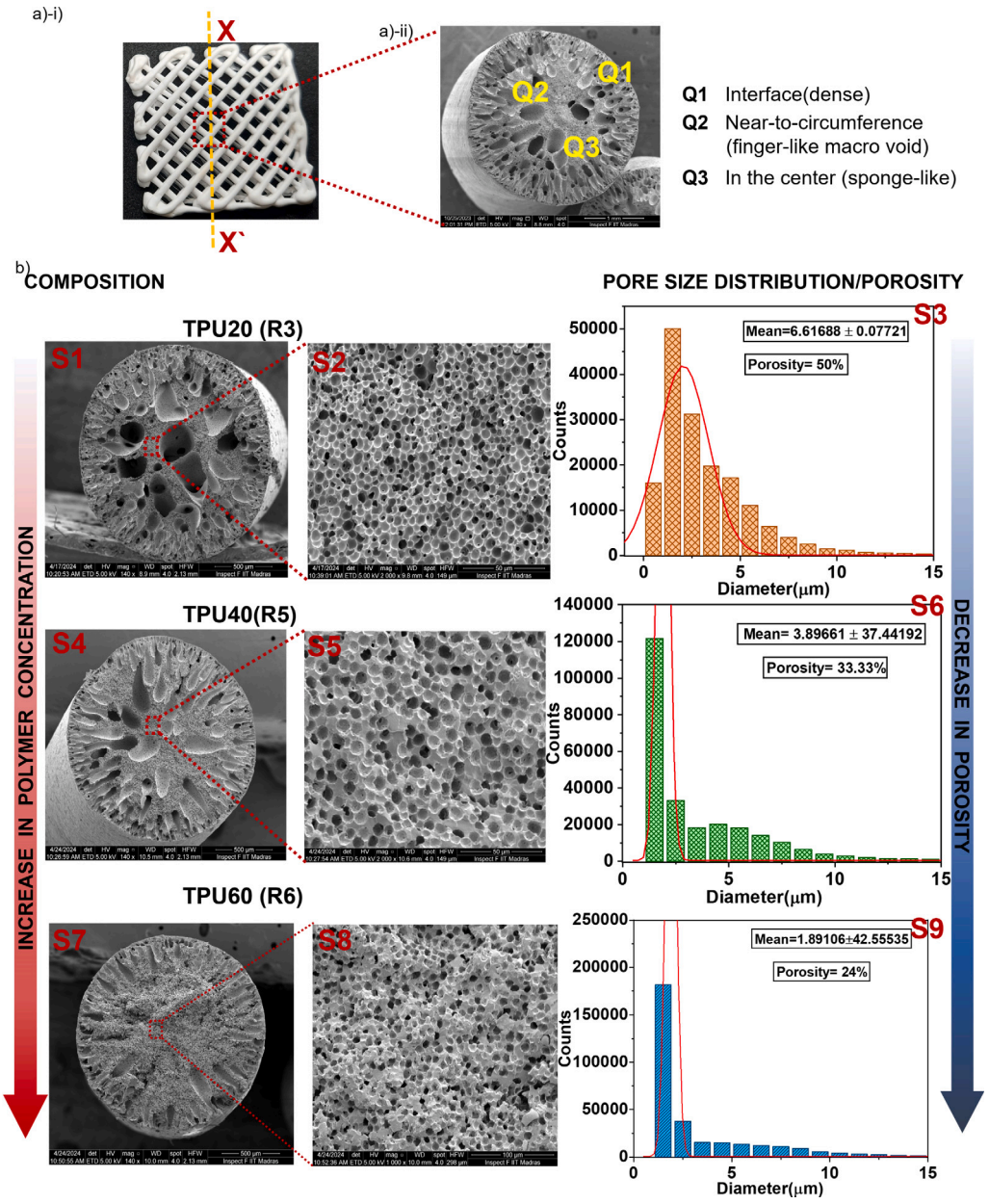

Fig. 7. (a)(i)Porous 3D printed grid-like structure, (a)(ii) SEM morphology of the cross-section of the 3D printed structure showing the dense non-porous interface and finger and sponge-like porous internal structure, (b) SEM images of the microstructure of the fracture surface of TPU printed structures by LLPS for varying concentration of TPU in DMF (20, 40, 60% w/v) with their pore size distribution and porosity analysis.

behaviour was observed for TPU30 to TPU70, as shown in Fig. 6, characterized by the decreasing viscosity over the increasing shear rate. The viscosities of the polymer inks varied in the range of 1–1000000 mPa s, which is lower compared to the ink used in DIW in air [4]. The ink with TPU compositions from 20%–60% w/v was used for printing different structures in our work.

3.4. Porous structures

Interestingly, this method of 3D printing resulted in strands with internal hierarchical pores. Fig. 7 summarizes the porous structures achieved by LLPS-3D printing. The porosity could be tailored by varying the polymer concentrations. The solutions of TPU in DMF (20%–60% w/v) were 3D printed at room temperature inside water.

The printed samples were treated with liquid nitrogen so as to fracture the structures at the cross-section. The cross-section of the printed structure revealed dense pores near the circumference, while the internal microstructure varied from finger-like cavities (macrovoid) to spherical (sponge-like) interconnected pores (as shown in Fig. 7a). The fingers formed were not uniform in their size, shape and physical dimensions. The difference in the microstructure was due to the liquid–liquid phase demixing rate (LLDR) at different positions of the extruded filament [21]. The duration between submerging the polymer ink in a coagulation bath and the point at which the solution becomes opaque was used to calculate the LLDR. Finger-like macrovoids were formed at the circumference of the filament due to higher LLDR as a result of instantaneous demixing. Whereas spherical sponge-like (or cellular-type) porous structures were obtained towards the centre of the filament due to delayed demixing (or phase separation) as evidenced by lower LLDR. The evolution of porous microstructure in the printed polymer structure was due to nucleation and growth of non-solvent droplets through LLPS. As discussed earlier, the aqueous TPU solution and water come into contact after the extrusion of the ink into the bath.

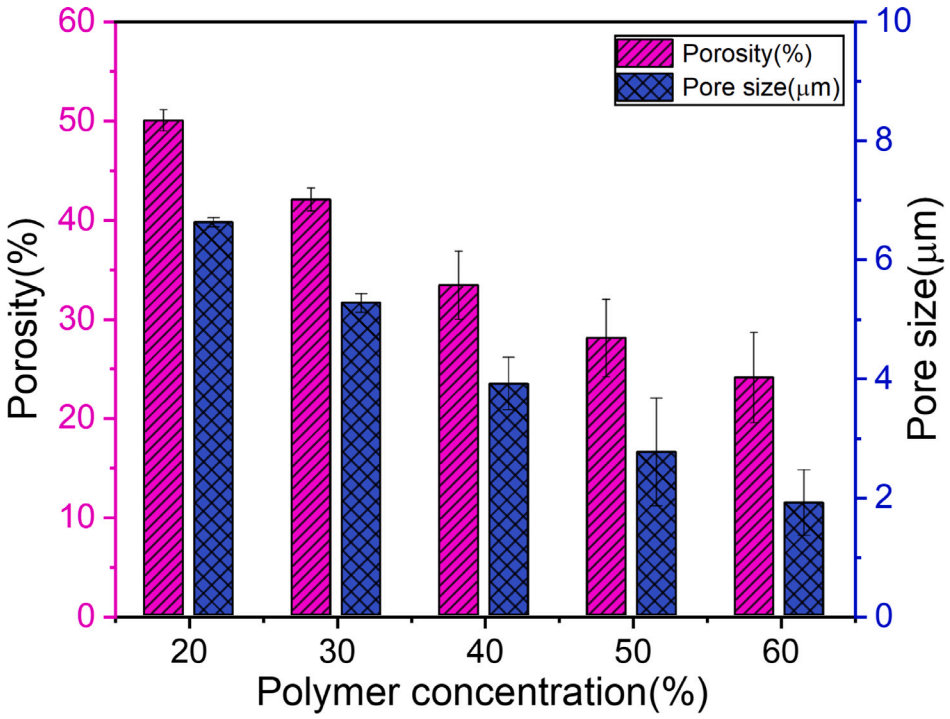

Fig. 8. The plot showing the pore characteristics of the printed strands with varying polymer concentration.

Due to the high miscibility of solvent and non-solvent, the mass transfer between the solvent and the non-solvent occurs at the interface.

The diffusion occurs radially from the outer surface to the centre of the filament. As the outer surface (point Q1 in Fig. 7(a-ii)) of the polymer filament was exposed to a higher quantity of water, the diffusion rate is higher compared to the centre. The higher diffusion in the periphery enhances the nucleation rate, leading to vitrification and crystallization over a shorter time period. As we move radially towards the centre (point Q2 and Q3 in Fig. 7(a-ii)), the nucleation rate is less, whereas the growth of nuclei formed is facilitated by continuous diffusion. Thus, the nucleation and growth does not occur at the outer surface of the printed structures. Hence, the outer surface of the structures was non-porous and dense. Phase separation is caused by the nucleation and development of the non-solvent droplets, and the non-solvent concentration in the TPU filament gradually increases on the inner surface (points Q2 and Q3 in Fig. 7(a-ii)). Because of this, the inner surface was porous while the outside surface was dense. In point Q2 of Fig. 7(a-ii), the size of the pores was found to be larger, suggesting the presence of a gradient in the pore size towards the centre. This implies that as the TPU volume increased, phase separation caused the water droplets to coalesce and grow larger as the diffusion of water into the outer surface (point Q1) was restricted. Hence, the pores generated near the surface point Q2 of the filament are bigger.

In general, the average porosity (effective volume fraction of pores) is influenced by the composition, particularly that of polymer. As the fraction of polymer composition decreases, the solvent/nonsolvent reaction is enhanced, resulting in increased porosity. The pore volume fraction corresponding to the selected composition in Fig. 4 is shown below, which conforms to the above assertion. R4 resulted in spherical (sponge-like) interconnected pores (as shown in Fig. 7(b), on the other hand, R2 showed that TPU structures have round sponge-like holes together with tapering and finger-like cavities (macrovoids). The distribution of porosity sizes in the printed TPU structures is depicted in Fig. 7. The equivalent diameter of the pores was calculated using the estimated area of the strands from the SEM image. A circularity of 0.6–0.9 was maintained throughout the image analysis using the ImageJ. The ink compositions that corresponded to point R2 yielded the strands with larger pores, whereas point R6 yielded the smallest pores. The Fig. 7b displays the cross-sectional scanning electron microscope (SEM) image of 3D printed TPU strands that were obtained using the ink composition in the regions R2, R5, and R6. Pore images at greater magnification are displayed in the insets of S2, S5, and S8. From these images, it is evident that TPU structures with distinct pore sizes were formed. Though the pore morphology in the strands with higher magnified regions look similar, spherical open cellular type (as shown in Fig. 7b for S2, S5, and S8), however, the pore size and pore density were different. Fig. 7b displays a comparison of the porosity and pore size (diameter) for the TPU strands that were produced by taking printing solutions with compositions in R2, R5, and R6. Pore size distribution was obtained from several SEM images of the cross-section of the printed strands, as shown in Fig. 7b S2, S5, and S8. While porosity was obtained by liquid displacement method using ethanol as solvent (explained in supplementary section S3). It was observed that printed strands from region R2 have pores of 6.617 ± 0.077 μm average diameter, with 50% porosity. On the other hand, structures from region R5 have smaller sizes (3.897 ± 37.442 μm) and less porosity ($\approx 33.33\%$) compared to structures prepared from ink in R2. However, the printed structures made from the ternary solutions corresponding to the area R6 showed pores of the smallest size (1.891 ± 42.555 μm) with denser (porosity$\approx$ 24%) structures. It was observed that the pore size and porosity decreased upon increasing the polymer concentration, as summarized in Fig. 8.

Uniaxial tensile tests were performed in a 1ST Tinius Olsen UTM (1kN). The tests were performed at a crosshead speed of 15 mm/min. All the experiments were repeated three times, and the average value was taken. The tensile strength was found to be 3, 3.49, 4, 4.96, and 8.32 MPa for 20%–60% w/v of TPU, respectively (see Fig. 9). The presence of in situ pores resulted in variations in the mechanical properties of the samples. With increase in polymer concentration, the tensile strength of the printed structures increased due to decrease in porosity. This type of soft and porous structure could find suitable applications in cell culture [12,13], tissue engineering scaffolds [14–16], and applications for EMI shielding [29,30]. The flexibility in altering the mechanical properties and microstructures is further helpful in designing complex structures for various applications.

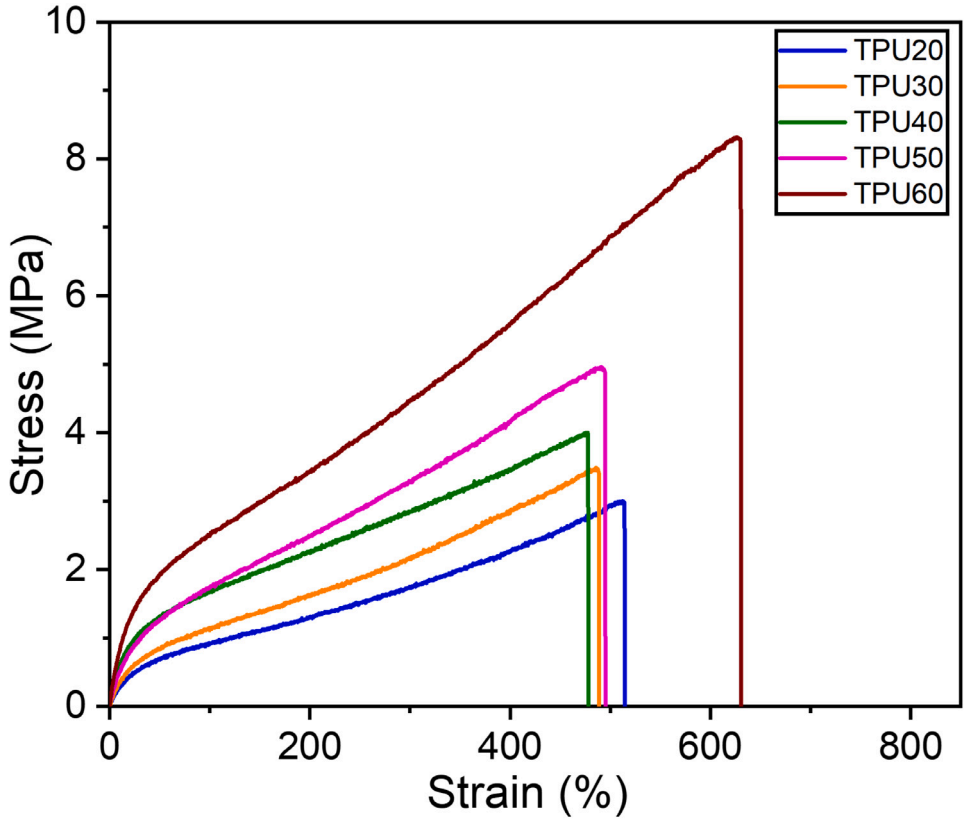

Fig. 9. Stress–strain curves of 3D printed TPU samples.

4. Application of printing under suspension media

In this work, two different printing strategies were analysed i.e., layer-by-layer approach and free-form building. DI water was used as suspension media for the former approach, and CMC gel was employed for the latter one, which served as a non-solvent for the TPU ink. The significance of the interfacial energy between the ink and the media (non-solvent) for LLPS-3D printing was emphasized by Karyappa et al. [27]. The capillary effect in the air caused the extrusion of TPU inks with low viscosity (like TPU20) to be discontinuous. However, with DI water, the same ink created a continuous filament (as explained in Section 3.3). The dispensing of the ink and the attachment of the printed filaments were unaffected by water, a Newtonian fluid. Structures printed in a DI water bath helped to achieve a buildability of 15 mm using soft polymer ink by rapid solidification of the ink. Different structures with varying layer heights were printed in water using TPU inks ranging from 20–50 %w/v. Grid or scaffold-like structures were printed with varying infill density and patterns (as shown in Fig. 10 and supplementary video SV2 & SV3). The printability studies correlate well with the single filament experiments discussed in the previous sections. A weak interlayer adhesion was observed with a low concentration of TPU (point R2 in Fig. 4b)) ink due to faster phase separation in non-solvent media. The interlayer adhesion increased with an increase in the concentration of TPU($\geq TPU30$, i.e., for the regions R2, R4, R5, and R6 in Fig. 4(b)) as expected due to lesser LLDR. Slowing down the rate of solidification provided better adhesion with the subsequent layer. Therefore, all the scaffold-like structures were printed with TPU50 ink, and the structures exhibited good shape fidelity in water (shown in Fig. 10 and movie SV3).

Deformation of soft structures upon layer-upon-layer addition is a major difficulty in the layer-by-layer technique used in conventional DIW-3D printing. Therefore, these are generally inadequate for fabricating free-form structures due to the low structural integrity with poor printing resolution in the z-direction. This necessitates the need for support structures in free-form constructs. The removal of the support structure, especially when printing soft materials, can potentially damage the structure.

Therefore, omnidirection printing was employed for continuous path printing of different helical structures (shown in figure S6). This method can overcome the above limitation by eliminating the necessity of support structures. To print a free-form structure, the suspension bath should exhibit certain characteristics. In addition to composition, the rheological characteristics of the medium should be compatible with the mixture.

However, the challenge in free-form 3D printing is the tuning of the rheological behaviour of the suspension media. The yield stress σ_y of the media should be sufficiently high to hold the extruded features. Similarly, the σ_y should not be high enough to resist the dispensing of the material from the nozzle. Another important rheological property of the media is the thixotropic time (usually <1s), i.e. the time scale of the reversible transition between the solid-like and liquid-like behaviour. The CMC gel offered a practical solution as suspension media as they behave as elastic solids at rest and exhibit shear-thinning behaviour under dynamic conditions. The shear-thinning behaviour of the gel was sensitive to the concentration of CMC powder from CMC1.0 to CMC6.0, as shown in Fig. 11 (CMC1.0 denoted 1w/v% of CMC, and the same nomenclature was used for other concentrations of CMC). Figure S3 shows that the CMC gel had finite yield strength and provided physical support for the printed structure. As the concentration of the CMC increased from CMC1.0 to CMC6.0, both σ_y and E_e linearly increased from 0.75 to 0.05 Pa and from 1.0 to 50 Pa, suggesting CMC6.0 as a good candidate to be used as suspension media for free-form structures. When low viscosity inks, like TPU20 and TPU30, are dispensed in low yield stress media, like CMC1.0 and CMC2.0, the dispensed ink adheres to the nozzle tip right away as the nozzle moves inside the bath. The supplementary video SV5 illustrates that the attached

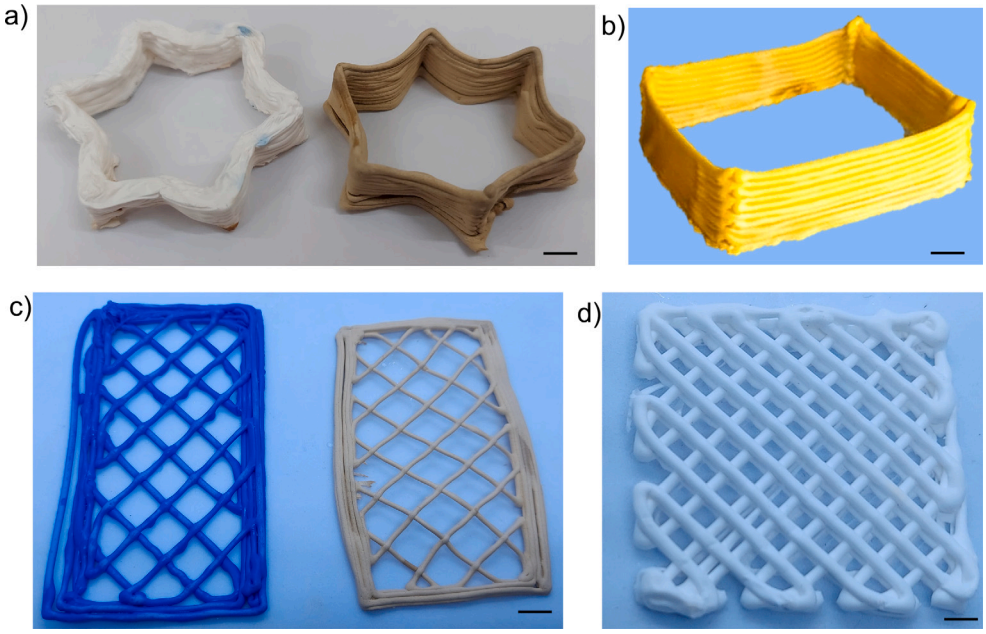

Fig. 10. (a) A star with 10 and 15 layers printed with TPU30 inside water without collapsing, (b) A square with 20 layers printed with TPU40 inside water without collapsing, (c)A grid-like structure printed with TPU50 with strong bonding at the junctions, (c) A scaffold structure printed in water (scale bar-1 cm).

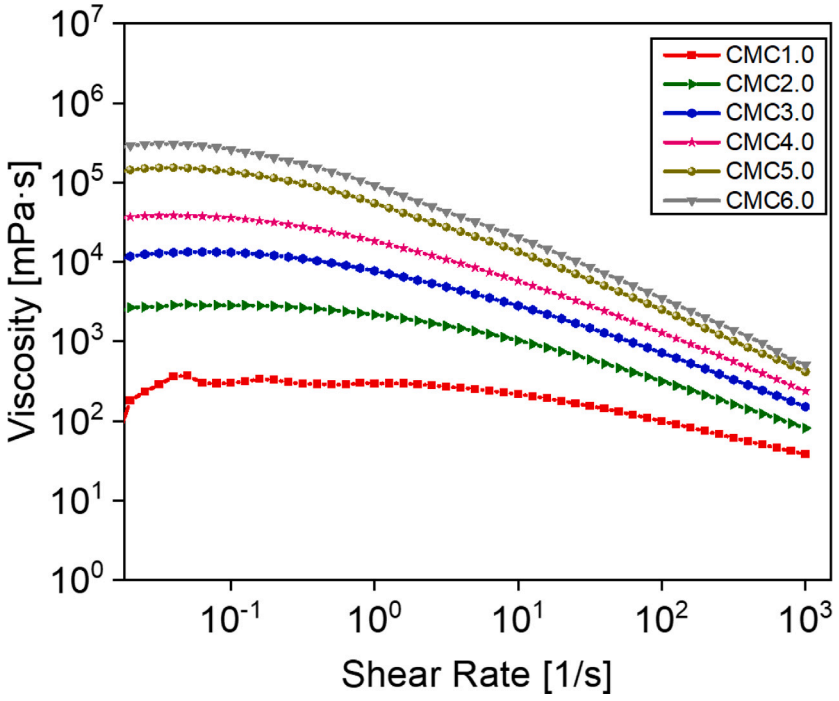

Fig. 11. A CMC gel showing shear thinning ability which acts as a supporting medium for free-form structures.

ink did not separate from the nozzle due to insufficient yield stress characteristics (σ_y and E_c) of CMC1.0 and CMC2.0. To resume printing in these situations, the collected ink had to be physically removed. The above problem was fixed once the ink and media's yield stress characteristics were increased (as shown in supplementary movie SV6). The printing parameters, along with the rheological characteristics of the media, were studied and optimized by printing a straight line in different media at a finite depth of the nozzle from the bottom. Different helical geometries were constructed under a suspension media as demonstrated in figure S3 and supplementary video SV7, SV8 & SV9.

5. Conclusions

The development of suspension bath 3D printing presents an innovative pathway in the fabrication of complex free-form architecture using soft materials. We demonstrated a 3D printing strategy using liquid–liquid phase separation for rapid curing of the polymer ink to develop porous structures. We are able to show the printability with the choice of different concentrations under equilibrium using the ternary phase diagram. In this work, water was used as a source of non-solvent for rapid solidification of TPU-DMF polymer ink. This method helped

to enhance the buildability of the printed structures. A viscous gel medium of CMC was employed for omnidirectional 3D printing of free-form constructs. This method served as a single-step fabrication process to achieve complex structures with internal hierarchical pores embedded in TPU. It was concluded that the mechanical properties of the structures could be modulated by altering the porosity. This work sheds light on the various processing factors needed for the effective 3D printing of intricate architectures from soft materials based on LLPS.

6. Abbreviations

TPU—Thermoplastic Polyurethane
DMF—Dimethyl Formamide
EMI—Electromagnetic Interference
DI—De-ionized
SEM—Scanning Electron Microscope

CRediT authorship contribution statement

Smruti Parimita: Writing – original draft, Validation, Methodology, Formal analysis, Data curation, Conceptualization. **Umamaheshwari Ravikumar:** Writing – review & editing, Methodology, Conceptualization. **Hariharan Krishnaswamy:** Writing – review & editing, Supervision. **Pijush Ghosh:** Writing – review & editing, Supervision, Resources, Funding acquisition, Formal analysis.

Declaration of competing interest

The authors declare that they have no known competing financial interests or personal relationships that could have appeared to influence the work reported in this paper.

Acknowledgments

“The authors would like to acknowledge the financial support from the Science and Engineering Research Board (SERB), Government of India, for supporting this work (Project No. CRG/2022/007942)”.

Appendix A. Supplementary data

Supplementary material related to this article can be found online at https://doi.org/10.1016/j.jmapro.2024.11.065.

References

[1] Dou Y, Luo J, Qi L, Lian H. A vertex-arc path planning method for metal droplet-based 3D printing of thin-walled parts with sharp corners. J Mater Process Technol 2023;312:117852.
[2] Diao Q, Zeng Y, Chen J. The applications and latest progress of ceramic 3D printing. Addit Manuf Front 2024;3(1):200113.
[3] Emon OF, Alkadi F, Kiki M, Choi J-W. Conformal 3D printing of a polymeric tactile sensor. Addit Manuf Lett 2022;2:100027.
[4] Parimita S, Kumar A, Krishnaswamy H, Ghosh P. Solvent triggered shape morphism of 4D printed hydrogels. J Manuf Process 2023;85:875–84.
[5] Moderator, Trimmer B, Participants, Lewis JA, Shepherd RF, Lipson H. 3D printing soft materials: what is possible? Soft Robot 2015;2(1):3–6.
[6] Zhou L-Y, Fu J, He Y. A review of 3D printing technologies for soft polymer materials. Adv Funct Mater 2020;30(28):2000187.
[7] Yan F, Zhou Q, Xu Y, Wang G, Li G, Ma C, Su G, Zhan X, Liu L. Learning from nature: constructing “rigid-soft” structure on carbon fibers surface by self-assembly to improve the performance of epoxy composites. Composites A 2024;176:107888.
[8] Rao S, Fan J, Zhou Y, Zeng X, Cheng X, Du G, Zeng X, Sun R, Ren L. High damping, soft and reprocessable thermal interface materials inspired by the microstructure of skin tissue. Compos Sci Technol 2024;247:110428.
[9] Venditto V, Vaiano V, Sacco O. Monolithic porous organic polymer-photocatalyst composites for applications in catalysis. ChemCatChem 2024;16(2):e202301118.
[10] Mandal A, Chatterjee K. The 3D/4D printing of polymeric scaffolds for bone tissue engineering. In: Emerging materials and technologies for bone repair and regeneration. CRC Press; 2025, p. 85–108.
[11] Kumar A, Rajamanickam R, Hazra J, Mahapatra NR, Ghosh P. Engineering the nonmorphing point of actuation for controlled drug release by hydrogel bilayer across the pH spectrum. ACS Appl Mater Interfaces 2022;14(50):56321–30.
[12] Huang R, Gao X, Wang J, Chen H, Tong C, Tan Y, Tan Z. Triple-layer vascular grafts fabricated by combined E-jet 3D printing and electrospinning. Ann Biomed Eng 2018;46:1254–66.
[13] Bergmeister H, Schreiber C, Grasl C, Walter I, Plasenzotti R, Stoiber M, Bernhard D, Schima H. Healing characteristics of electrospun polyurethane grafts with various porosities. Acta Biomater 2013;9(4):6032–40.
[14] Cutiongco MF, Anderson DE, Hinds MT, Yim EK. In vitro and ex vivo hemocompatibility of off-the-shelf modified poly (vinyl alcohol) vascular grafts. Acta Biomater 2015;25:97–108.
[15] Kharazi AZ, Atari M, Vatankhah E, Javanmard SH. A nanofibrous bilayered scaffold for tissue engineering of small-diameter blood vessels. Polym Adv Technol 2018;29(12):3151–8.
[16] Wang W, Nie W, Zhou X, Feng W, Chen L, Zhang Q, You Z, Shi Q, Peng C, He C. Fabrication of heterogeneous porous bilayered nanofibrous vascular grafts by two-step phase separation technique. Acta Biomater 2018;79:168–81.
[17] Yang X-Y, Chen L-H, Li Y, Rooke JC, Sanchez C, Su B-L. Hierarchically porous materials: synthesis strategies and structure design. Chem Soc Rev 2017;46(2):481–558.
[18] Montazerian H, Mohamed M, Montazeri MM, Kheiri S, Milani A, Kim K, Hoorfar M. Permeability and mechanical properties of gradient porous PDMS scaffolds fabricated by 3D-printed sacrificial templates designed with minimal surfaces. Acta Biomater 2019;96:149–60.
[19] Pervin R, Ghosh P, Basavaraj MG. Tailoring pore distribution in polymer films via evaporation induced phase separation. RSC Adv 2019;9(27):15593–605.
[20] Pervin R, Ghosh P, Basavaraj MG. Engineering polymer film porosity for solvent triggered actuation. Soft Matter 2021;17(10):2900–12.
[21] Pervin R, Ghosh P, Basavaraj MG. Influence of initial composition of casting solution on morphology of porous thin polymer films produced via phase separation. J Polym Res 2022;29(11):486.
[22] Rizvi R, Naguib H. Porosity and composition dependence on electrical and piezoresistive properties of thermoplastic polyurethane nanocomposites. J Mater Res 2013;28(17):2415–25.
[23] Yu X, Yuan H, Pan Z, Pan H, Chu H, Li D. Porous nano-grained cuprous selenide (Cu2Se) for mid-infrared photonics. J Alloys Compd 2024;987:174179.
[24] Jiang J, Zheng H, Liu H, Zhai W. Tunable cell structure and mechanism in porous thermoplastic polyurethane micro-film fabricated by a diffusion-restricted physical foaming process. J Supercrit Fluids 2021;171:105205.
[25] Kim TH, Kim M, Kim EJ, Ju M, Kim JS, Lee SH. Highly stretchable thermoplastic polyurethane separators for Li-ion batteries based on non-solvent-induced phase separation method. Polymers 2024;16(3):357.
[26] Mandel RM, Lotlikar PS, Keasler KT, Chen EY, Wilson JJ, Milner P. Gas delivery relevant to human health using porous materials. Chem Eur J 2024;e202402163.
[27] Karyappa R, Ohno A, Hashimoto M. Immersion precipitation 3D printing (ip 3DP). Mater Horiz 2019;6(9):1834–44.
[28] Karyappa R, Ching T, Hashimoto M. Embedded ink writing (eiw) of polysiloxane inks. ACS Appl Mater Interfaces 2020;12(20):23565–75.
[29] Menon AV, Madras G, Bose S. Shape memory polyurethane nanocomposites with porous architectures for enhanced microwave shielding. Chem Eng J 2018;352:590–600.
[30] Menon AV, Jagadeshvaran P, Bose S. Geometry and mesh size control the EMI shielding in 3D printed conducting shape memory PU structures. J Mater Chem C 2023;11(13):4474–85.
[31] Guillen GR, Pan Y, Li M, Hoek EM. Preparation and characterization of membranes formed by nonsolvent induced phase separation: a review. Ind Eng Chem Res 2011;50(7):3798–817.
[32] Denolf R, Hogie J, Figueira FL, Mertens I, De Somer T, D’hooge DR, Hoogenboom R, De Meester S. Constructing and validating ternary phase diagrams as basis for polymer dissolution recycling. J Mol Liq 2023;387:122630.
[33] Baru S-i, Matthews S, Marchese E, Walsh P, Coffey A. The effect of sub-and near-critical carbon dioxide assisted manufacturing on medical thermoplastic polyurethane. Polymers 2023;15(4):822.